

SM Metals Park, Ohio, pp. 37-45.

ina-Reinforced Composites," *ASTM STP 546*, pp.

Unidirectional Composites under Compressive  
J. V. Tamuzs, eds., The Hague: Martinus Nijhoff  
of Long-Fibre Unidirectional Composites," *J.*

ive Response of Kevlar/Epoxy Composites," *J.*

Fiber Waviness on the Compressive Strength of  
*Mat. & Struct.*, pp. 120-125.

Compressive Failure of Weakly Bonded Fiber-  
*ls.*, 22:818-828.

mechanical Modelling of Composite Compressive

odel for *in-situ* Compression Strength of Fiber  
14:8-12.

ssive Failure of Fibre Composites due to Micro-  
*ation of Composite Materials*, Springer-Verlag,

ressive Failure of Fibre Composites," *J. Mech.*

mparison between Compressive Strength due to  
sites," *ECCM 8 Conf. Proc.*, p. 35 E.

Compressive Failure due to Kinking of Fibrous  
6.

Compressive Strength of Thick-Section Advanced  
, 25:1244-1276.

etween Fibre Divagation and Compressive Pro-  
*Symp.*, pp. 2236-2244.

in Thick Composites and Its Effect on Their  
p. 30-F.

Wilkins. 1992. "Kink Failure Analysis of Thick  
*aterials*, 27:471-490.

fections in Unidirectionally Reinforced Compos-

onstituents Requirements to Improve Composites  
. pp. 544-558.

iviness on the Relationship between Compressive  
posites," *J. Composite Materials*, 28:66-76.

y. 1992. "A Parametric Study of Variables That  
posite Laminates: Part 1—Analysis," *J. Composite*

mina Longitudinal Compression Strength of Car-  
*ce Materials*, 30:1115-1131.

ject Contr. No. BRE2-CT92-0314.

echanics and Plastic Analysis or Limit Design,"

990. Technomic Pub. Co., Inc.

## Bond Behavior of Deformed GFRP Rebars

M. R. EHSANI, H. SAADATMANESH AND S. TAO  
*Department of Civil Engineering and Engineering Mechanics*  
*The University of Arizona*  
*Tucson, AZ 85721*

(Received October 13, 1995)  
(Revised September 16, 1996)

**ABSTRACT:** The bond behavior of straight Glass-Fiber-Reinforced-Plastic (GFRP) reinforcing bars to concrete was experimentally investigated. Results of 48 beam and 18 pull-out specimens constructed with No. 3, 6, and 9 GFRP rebars are presented. The static tensile load was applied to the rebars in a gradual increment of load level until splitting failure of concrete, rebar pull out failure, or rebar fracture occurred. The slip between the rebars and concrete was measured at the loaded and free ends at each load level. Variables in the study included concrete compressive strength, embedment length, clear concrete cover, rebar diameter, and concrete cast depth. On the basis of the experimental results, it was concluded that the ultimate bond stress increases with higher concrete compressive strength and clear concrete cover, but decreases with larger concrete cast depth. The ultimate bond stress and the loaded end slip of the pull-out specimens were found to be greater than that of the beam specimens. Beam test data could be more realistic and accurate for use in determining the development length.

**KEY WORDS:** Glass-Fiber-Reinforced-Plastic (GFRP), rebar, bond strength, reinforced concrete, development length, anchorage.

### INTRODUCTION

CONCRETE REINFORCED WITH steel reinforcing bars is widely used in a variety of construction projects such as bridge decks, parking garages, etc. However, corrosion of reinforcing steel is a particularly serious problem in structures located in aggressive environments. Rust from corroded rebars occupies a larger volume than the iron from which it is formed. This results in large internal pressures which lead to cracking and spalling of concrete. With time, deep pitting and a severe loss of cross section of the reinforcing steel can take place. A combination of high stress and intense corrosion may lead to costly repairs or catastrophic failure of the structure.

Several methods have been developed and used to prevent corrosion of steel

reinforcement such as the use of additives and admixtures to improve the impermeability of concrete and the use of epoxy-coated steel rebars. The latter has been used extensively in bridges and parking structures. However, in many cases, the coating can be damaged during construction, allowing moisture to penetrate the coating and reach the steel bar. The recent discovery of extensive premature corrosion of epoxy-coated steel rebars in new bridges points to the shortcomings of this technique (Kessler and Powers, 1988). While these studies are not conclusive enough to call for a discontinuation of the use of epoxy-coated bars, there is a growing interest in developing more durable materials as replacement for steel rebars for construction in severe environments.

Glass-Fiber-Reinforced-Plastic (GFRP) rebars which have been produced in recent years appear to be a suitable candidate and have great potential to fill such a need. These rebars have several important advantages over conventional reinforcing steel, namely, high corrosion resistance, high tensile strength, high strength-to-weight ratio, nonconductivity, ease of handling and cutting, and economy (Ehsani, 1993). While glass fibers are highly resistant to corrosion by acids, the combination of the wrong types of fibers and resins could lead to premature deterioration of GFRP bars in alkaline environment such as that in fresh concrete (Sen et al., 1993). However, many structures constructed with these bars have been in service for more than ten years in extremely aggressive environments with no sign of deterioration of the rebars (ACI Committee 440, 1996).

There are a number of issues related to the behavior of FRPs which need to be addressed. Among these are the larger deflections caused by the lower modulus of elasticity of FRPs, creep rupture of the fibers at relatively low sustained stresses, fire resistance, etc. Another factor limiting the use of GFRP rebars is the lack of information and design guidelines on their bond to concrete. Pleimann conducted pull-out tests and reported that the bond strength of the rebars improved with bar diameter (Pleimann, 1987 and 1991).

Faza and GangaRao (1990) investigated the bond behavior of GFRP rebars by testing cantilever beams and pullout specimens. The results indicated that the decrease in the bond strength with increasing embedment length was attributed to the increase in the perimeter area of the rebars.

In another study by Chaallal, et al. (1992), pullout tests were undertaken to evaluate bond strength as well as development length of glass fiber composite rods embedded in normal strength concrete (NSC) and high strength concrete (HSC). Development length was defined as the minimum embedded length required to develop the ultimate tensile force,  $T_u$ , of the rod. It was concluded that development length is approximately twenty times the bar diameter for both NSC and HSC.

Bond strength of glass-fiber-reinforced-plastic rebars was experimentally investigated by Daniali (1992). A total of 30 concrete beams were tested and results showed that a development length of 203 mm (8 in) was adequate for developing the ultimate tensile strength of a No. 4 bar. The full strength of a No. 6 bar could be developed over 457 mm (18 in) of embedment length if shear reinforcement was provided along the entire length of the specimen. Still, the lack of sufficient

information about bond behavior of GFRP rebars to concrete limits their use in field applications.

In one of the first reported studies on FRP-reinforced concrete beams, the behavior of five rectangular beams and one T-beam reinforced with GFRP rebars was presented (Saadatmanesh and Ehsani, 1991). Based on the relatively large number of narrow cracks in the beams, it was concluded that bond between the GFRP rebars and concrete was good. No failure was observed due to debonding of the rebars and concrete. This study is a continuation of that investigation with the principal objective of examining the bond behavior of straight and hooked GFRP rebars to concrete. A total of 102 specimens have been tested. Based on the experimental results, the analytical study focused on the derivation of design equations, i.e., basic development length expressions for straight and hooked GFRP rebars. Due to space limitation, this paper will discuss the study of the bond behavior of straight GFRP rebars to concrete only. The study on bond behavior of hooked GFRP rebars to concrete, and the development of design guidelines for bond of GFRP rebars to concrete have been presented elsewhere (Ehsani et al., 1995 and 1996).

## RESEARCH SIGNIFICANCE

There is a growing interest in the use of composite rebars which can lead to more durable structures. However, the lack of data on bond performance has limited the field application of these materials. The findings of this study should be of interest to design engineers, manufacturers, and those involved in development of code provisions.

## EXPERIMENTAL PROGRAM

The primary objectives of the research program discussed here were to investigate the influence of several parameters on bond behavior of straight GFRP rebars to concrete. Forty-eight beam specimens and 18 pull-out specimens were constructed and tested. Variables in both beam and pull-out tests were concrete compressive strength, embedment length, clear concrete cover, rebar diameter, and concrete depth below the bar. For both beam and pull-out tests, the collected data included ultimate load under static loading, ultimate bond stress, slip at loaded and free ends, mode of failure, and load-slip relationships.

### Design and Construction of Specimens

The specimens were divided into two groups, i.e., beam specimens, and pull-out specimens. The test specimens are shown in Figure 1, and the dimensions of beam specimens are listed in Table 1. It has been suggested that the bond strength of rebars is affected by the unbonded lead length of the bar (Hadje-Ghaffari, et al., 1992). To eliminate this effect, the leading 76 mm (3 in) of each rebar was covered with a thin conduit to prevent its bonding to concrete (Figure 1). The unbonded region near the free end of each bar was varied so that the desired bonded length,  $L$ , could be obtained. Each beam specimen contained two bars

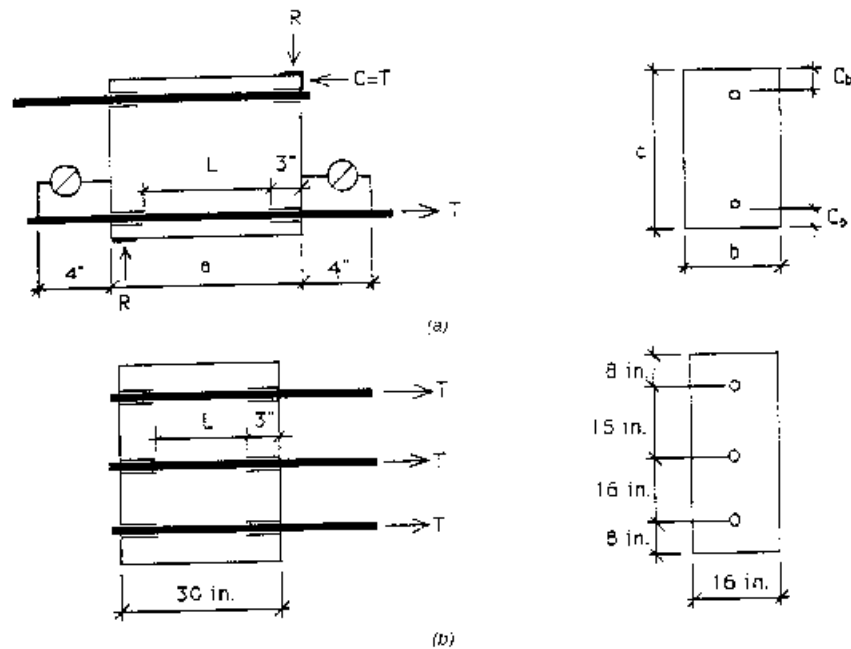


Figure 1. Test specimens: (a) View of beam specimens; (b) View of pull-out specimens.

[Figure 1(a)], resulting in two separate test specimens. Each pull-out specimen contained three bars [Figure 1(b)]. Thus, six concrete blocks were constructed to obtain the 18 test specimens.

The concrete was placed in several lifts, and each layer was compacted with the aid of an electrical vibrator. Sixteen  $152 \times 305$  mm ( $6 \times 12$  in) test cylinders were cast from each batch. They were cured under the same condition as the specimens. At the end of casting, the top surfaces of all specimens and cylinders were covered with plastic sheets, and allowed to cure for 7 days. At that time, the plywood forms were removed and the specimens and cylinders were stored under the same environmental condition until the day of testing. All specimens were older than 28 days at the time of testing.

Table 1. Dimensions of beam specimens.

Rebar Size	Nominal Rebar Diameter (mm)	a (mm)	b (mm)	c (mm)
No. 3	10	355	255	355
No. 6	19	610	510	610
No. 9	19	915	510	760

### Material Properties

Two batches of concrete were ordered from a local ready-mix plant. The mixes were designed to provide a minimum 28-day compressive strength of 28 and 56 MPa (4000 and 8000 psi). Maximum size of the concrete aggregate was 25 mm (1 in).

The GFRP rebars used in the tests were supplied by a U.S. manufacturer. The volumetric fraction of the E-glass fibers was approximately 72%; the other constituent material in the rebar was a polyester resin matrix which occupied about 28% of the volume. No. 3, 6, and 9 GFRP rebars were used in this study (Figure 2). During manufacturing, the longitudinal fibers are wrapped in a helical pattern with a small strand of fibers to induce deformations on the bar and to improve its bond behavior. The width of the strand is usually the same for all rebar sizes. As shown in Figure 3, the pitch is defined as the distance from the center to center of strands. Larger diameter rebars had longer pitches.

Although most manufacturers produce GFRP rebars in the same diameters as steel rebars, there are no standard sizes for composite rods. Due to this lack of standards, non-uniformities usually exist in the physical dimensions of GFRP rebars. Some rebars may even have cross sections that are slightly oval shaped rather than a true circle (Ehsani, 1993). Representative 152 mm (6 in) long rebar samples were cut and submerged in a graduated cylinder to measure their volumes. Rebar diameters were then calculated from these values assuming a circular cross section for the bars. These measurements are slightly different from the nominal values (Table 2). Rib heights were calculated as an average of one half of the difference between the largest and smallest diameters for several points along the sample. The results are also presented in Table 2.

The ultimate tensile strength and the modulus of elasticity of GFRP rebars were measured based on the average values from uniaxial tension tests of three coupons for each bar size. A linear stress-strain relation for the entire range of

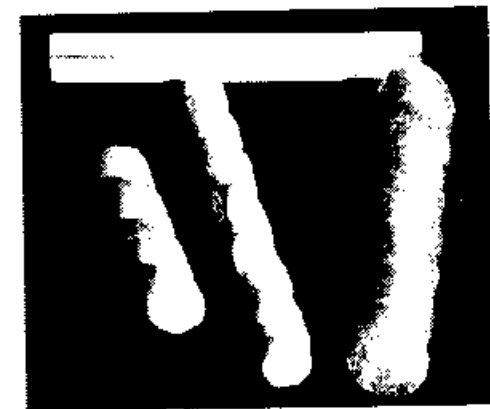


Figure 2. No. 6, 3, and 9 GFRP rebars used in the study.

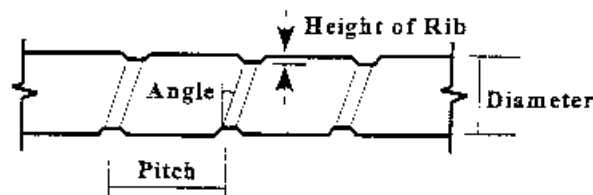


Figure 3. Sample for measuring rib geometry.

loading was obtained for all tension tests. The average ultimate tensile strengths for No. 3, 6, and 9 bars were 931, 641, and 531 MPa (135, 93, 77 ksi), respectively. The average modulus of elasticity for No. 3, 6, and 9 bars were 46950, 48610, and 50200 MPa (6810, 7050, and 7280 ksi), respectively.

The design and development of suitable grips to test GFRP rebars in tension have presented some difficulties. Because glass fiber based composites are very weak for loads applied transverse to the fiber direction, the region of the GFRP rebar in the grip must be protected against crushing. The grip must grasp the rebars in a manner as to avoid failure of the rebar at the grips, allowing the failure to take place in the rebar away from the grip region (Faza and GangaRao, 1990). A specially constructed set of sand-coated grips similar to those used in testing of GFRP rebars at West Virginia University were employed. The applied loads are transmitted from the jack to the GFRP rebars through these grips. The tests were successful in avoiding excessive slippage and/or rebar failure in the grips for all rebar sizes.

The modulus of elasticity for GFRP rebars is almost constant and averages about 48270 MPa (7000 ksi). However, the results point out that the tensile strength decreases with an increase in the rebar diameter. This reduction in strength is attributed to the "shear lag" phenomenon associated with the tensile force resistance of the core fibers and those at the contact surface of the rebars and the grips (Wu, 1991). The Poisson's ratio for GFRP bars has been reported to be 0.28 (Chaallal et al., 1992) which is close to that for steel. Therefore, little if any changes between the bond behavior of steel and GFRP can be attributed to the Poisson's ratio.

Table 2. Rib geometry of GFRP rebars.

Property	No. 3	No. 6	No. 9
Rib Height, mm	1.1	1.3	2.0
Pitch, mm	17.5	23.8	27.0
Angle, Degree	37	25	23
Measured Diameter, mm	9.7	18.4	27.4
Nominal Diameter, mm	10	19	29



Figure 4. Test set up for beam specimens.

### Test Set Up and Instrumentation

The beam specimens were tested in the steel reaction frame shown in Figure 4. This test set up resulted in a state of stress similar to that in a concrete beam, i.e., compression in the top of the section while the GFRP bar is under tension. However, for pull-out tests shown in Figure 5, the jack was in direct contact with the surface of the specimens, applying a compressive reaction force to the concrete block (Ehsani, et al., 1993).

Due to the low shear strength of GFRP rebars, care must be taken not to harm the rebars during the handling of the specimens and their positioning in the test frame. The tensile load was applied to the rebars using a hydraulic jack. The specimens were loaded under static loading and in a gradual increment of load

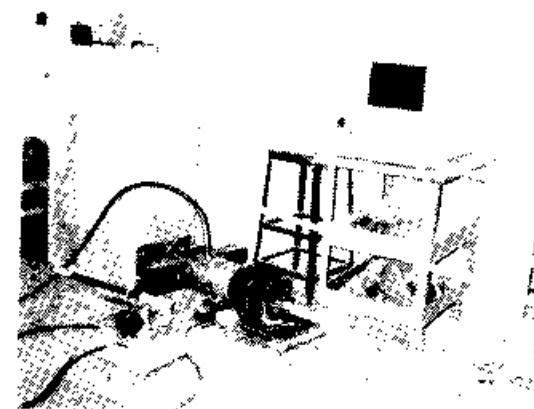


Figure 5. Test set up for pull-out specimens.

level until splitting of concrete, rebar pull out, or fracture of rebar occurred. The applied load was monitored by a load cell and the results were automatically recorded and printed at predetermined intervals. At each load increment, the slip between the rebar and concrete was recorded at the loaded and free ends of the rebar. As seen in Figure 1(a), this was obtained through dial gages which were attached to the loaded- and free-ends of the rebar.

### TEST RESULTS

The bond behavior of straight GFRP rebars to concrete was studied through testing of 66 specimens. The measurements of the load values and slips at loaded and free ends were taken at each increment of static loading. The load values were used to determine the corresponding bond stress. Bond stress is defined as the shear force per unit surface area of the rebar, and computed as

$$u = \frac{T}{\pi d_s l_d} \quad (1)$$

where,  $u$  = bond stress,  $T$  = applied tension force,  $d_s$  = diameter of the rebar, and  $l_d$  = embedment length.

A typical curve representing the load values versus slips at loaded and free ends for Specimen 46B18T6 is shown in Figure 6. Obviously, the slip at the loaded end is significantly larger than that at the free end. The loaded-end slip in-

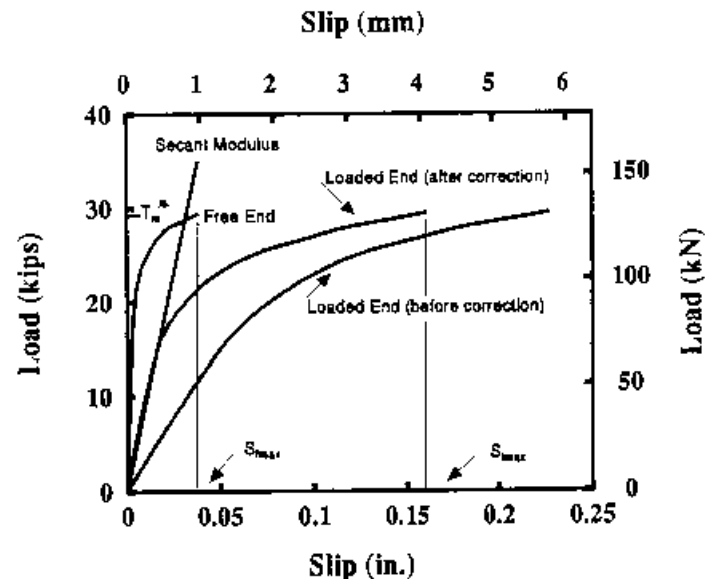


Figure 6. Typical load vs. slip relationship.

creased with the increase of load values at the beginning of the loading. However, the free-end slips would not take place until the adhesion resistance between the rebar and concrete was broken.

As shown previously in Figure 1(a), the dial gage attached to the loaded end of the rebar measured the movement of a point 102 mm (4 in) away from the concrete block relative to the face of the block. In addition, the first 76 mm (3 in) of the rebar was always shielded to prevent its bonding to concrete. Therefore, the measured slip at the loaded end of the rebar included the elastic elongation of the 178 mm (7 in) lead length. Due to the low modulus of elasticity of GFRPs, this elongation is significant and had to be corrected for. Thus, the actual slip,  $\delta_a$ , was calculated as the difference between the measured slip at the loaded end,  $\delta_m$ , and the elastic deformation,  $\delta_e$ .

The test data for beam specimens and pull-out specimens are given in Tables 3 and 4, respectively. The notation for beam specimens is as follows: the first number indicates the concrete compressive strength in units of ksi; the second number, the rebar diameter; the letter "B" for beam specimen; the fourth number, the embedment length in inches; the next letter designates the rebar casting position, T: Top, and B: Bottom; and the last number, the ratio of the clear concrete cover to rebar diameter. For instance, 43B1.5T1 was a beam specimen cast with 28 MPa (4000 psi) concrete, No. 3 GFRP rebar, 38 mm (1.5 in) embedment length, top rebar, with a clear concrete cover of one rebar diameter.

For pullout specimens, the first number represents the concrete compressive strength; the second, the rebar diameter; the letter "P" to designate a pull-out specimen; the next character identifies the rebar casting position; B: Bottom, M: Middle, T: Top, and the last number is the embedment length in inches. As shown in Figure 1, all pull-out specimens had very large clear covers on all sides.

In order to eliminate the effects of the minor variation in the concrete compressive strength for the 28 and 56 MPa (4000 and 8000 psi) specimens, it was decided to normalize the results with respect to the average concrete compressive strength for each group. The procedure carried out was as follows. For each group of specimens which were tested at approximately the same age, three concrete cylinders were tested in compression. For example, for Specimens 43B1.5T1, 43B1.5T2, and 43B3T2, three cylinders were tested which resulted in an average compressive strength of 27.65 MPa (4010 psi). This value is reported in the second column of Table 3 for these three specimens. Next, an average compressive strength,  $f'_{con}$ , was calculated for all specimens with nominal concrete strength of 28 or 56 MPa (4000 or 8000 psi). These averages were 33 MPa (4810 psi) and 47 MPa (6820 psi), respectively.

It is widely accepted that bond failure is proportional to tensile strength of concrete (Ferguson and Thompson, 1962). Since the tensile strength of concrete is proportional to the square root of its compressive strength, bond expressions also include the  $\sqrt{f'_c}$  term (ACI 318-95). For ease of comparison, the maximum load and bond stresses reported in columns 3 and 4 of Tables 3 and 4 have been multiplied by the factor  $\sqrt{f'_{con}/f'_c}$  and reported as  $T_m^*$  and  $u_m^*$ , respectively. This eliminated any influence the changes in  $f'_c$  might have on further analysis of the test results.

Table 3. Test data for beam specimens.

Specimen	$f'_c$ MPa	$T_m^*$ kN	$u_m^*$ MPa	$T_m^*/T_u$	$S_{fmax}$ mm	$S_{lmax}$ mm	$E_i$ kN/mm	Failure Mode
43B1.5T1	27.65	24.9	21.85	0.50	0.47	1.53	54.6	S
43B1.5T2	27.65	31.1	27.31	0.63	0.34	1.13	113.1	P
43B3T2	27.65	33.8	14.62	0.68	0.62	1.95	114.5	P
43B4B2	29.86	36.0	11.85	0.73	0.09	0.50	102.8	R
43B4T2	29.86	39.1	12.87	0.79	0.10	0.53	83.0	R
43B6B4	35.03	43.1	9.46	0.87	0.10	0.54	105.9	R
43B6T4	35.03	38.7	8.49	0.78	0.11	0.56	89.3	R
43B8B6	35.03	45.4	7.46	0.92	0.10	0.62	112.3	R
43B8T6	35.03	38.3	6.29	0.77	0.10	0.64	96.1	R
83B4B2	48.95	36.5	12.00	0.74	0.14	0.63	92.8	R
83B4T2	48.95	39.1	12.87	0.79	0.16	0.66	81.3	R
83B6B4	48.95	42.3	9.27	0.86	0.10	0.52	106.8	R
83B6T4	48.95	36.9	8.09	0.75	0.11	0.56	95.6	R
83B8B6	48.95	37.4	6.14	0.76	0.08	0.52	147.6	R
83B8T6	48.95	42.3	6.95	0.86	0.08	0.54	111.0	R
46B3B1	27.65	66.7	14.63	0.51	1.33	5.07	158.8	S
46B3T1	27.65	53.4	11.71	0.41	1.62	5.05	112.6	S
46B3B2	27.65	85.4	18.73	0.65	1.15	2.27	218.9	P
46B3T2	27.65	71.2	15.61	0.54	1.25	4.81	179.1	P
46B6B2	27.65	96.5	10.14	0.71	0.66	2.43	211.5	P
46B6T2	27.65	75.6	8.29	0.58	1.21	3.57	165.3	P
46B12B2	39.16	94.3	5.17	0.72	0.88	3.41	217.5	P
46B12T2	39.16	88.1	4.83	0.67	1.53	2.80	189.1	P
46B16B4	39.16	121.3	5.01	0.93	1.52	4.54	199.8	P
46B16T4	39.16	114.8	4.72	0.88	1.77	5.36	149.6	P
46B18B6	39.16	128.5	4.70	0.98	0.88	3.65	149.0	R
46B18T6	39.16	130.8	4.78	1.00	0.98	4.28	143.2	R
86B12B2	47.71	102.7	5.63	0.78	1.72	4.75	252.9	P
86B12T2	47.71	99.6	5.46	0.76	2.23	5.07	216.7	P
86B16B4	47.71	125.4	5.16	0.96	1.43	4.54	205.8	P
86B16T4	47.71	120.1	4.94	0.92	1.59	4.40	158.7	P
86B18B6	47.71	133.9	4.90	1.02	0.75	3.95	225.2	R
86B18T6	47.71	130.8	4.78	1.00	0.83	4.32	177.2	R
49B4B1	27.65	109.4	12.00	0.47	1.16	5.41	331.1	S
49B4B2	27.65	155.7	17.07	0.67	1.44	5.87	697.0	P
49B8B2	27.65	173.5	9.51	0.75	1.44	5.03	432.4	P
49B22B2	39.72	196.2	3.91	0.84	1.07	4.20	529.0	P
49B22T2	39.72	192.2	3.83	0.83	2.61	3.76	342.1	P
49B26B4	39.72	213.9	3.61	0.92	1.43	5.36	601.5	P
49B26T4	39.72	205.1	3.46	0.88	2.23	7.07	416.1	P
49B30B6	39.72	227.7	3.33	0.98	1.19	3.17	518.3	R
49B30T6	39.72	230.4	3.37	0.99	1.47	3.59	326.1	R
89B22B2	44.75	204.6	4.06	0.88	1.16	4.42	516.6	P
89B22T2	44.75	196.2	3.91	0.84	2.06	5.04	335.5	P
89B26B4	44.75	221.1	3.73	0.95	1.71	5.14	579.8	P
89B26T4	44.75	213.1	3.59	0.92	1.37	6.33	428.2	P
89B30B6	44.75	230.9	3.37	0.99	0.94	3.02	499.3	R
89B30T6	44.75	240.2	3.51	1.03	1.02	3.08	357.9	R

Table 4. Test data for pull-out specimens.

Specimen	$f'_c$ MPa	$T_m^*$ kN	$u_m^*$ MPa	$T_m^*/T_u$	$S_{fmax}$ mm	$S_{lmax}$ mm	$E_i$ kN/mm	Failure Mode	Top Bar Ratio
43PB1.5	32.2	33.4	29.3	0.68	0.21	1.30	93.5	P	1.00
43PM1.5	32.2	32.0	28.1	0.65	0.37	1.58	73.9	P	1.04
43PT1.5	32.2	31.6	27.7	0.64	0.39	1.69	70.9	P	1.06
83PB6	45.8	48.5	10.6	0.98	0.07	0.61	120.4	R	1.00
83PM6	45.8	42.7	9.4	0.86	0.08	0.64	98.0	R	1.14
83PT6	45.8	40.5	8.9	0.82	0.08	0.64	95.9	R	1.20
46PB6	32.2	105.9	11.6	0.81	0.99	4.35	193.0	P	1.00
46PM6	32.2	89.0	9.8	0.68	1.25	5.05	153.7	P	1.19
46PT6	32.2	85.8	9.4	0.65	1.19	5.08	153.3	P	1.23
86PB12	45.8	120.5	6.6	0.92	1.16	5.37	239.1	P	1.00
86PM12	45.8	110.8	6.1	0.84	2.26	6.79	221.9	P	1.09
86PT12	45.8	106.3	5.8	0.81	2.53	7.06	220.2	P	1.13
49PB8	32.2	213.1	11.7	0.92	1.66	7.31	305.9	P	1.00
49PM8	32.2	187.7	10.3	0.81	1.99	7.59	205.1	P	1.13
49PT8	32.2	185.9	10.2	0.80	2.00	8.40	203.4	P	1.15
89PB22	45.8	219.3	4.4	0.94	1.51	5.36	519.2	P	1.00
89PM22	45.8	203.7	4.1	0.88	2.22	8.17	283.0	P	1.08
89PT22	45.8	200.2	4.0	0.86	2.17	7.92	282.3	P	1.09

The fifth column in Tables 3 and 4 includes the ratio of  $T_m^*/T_u$ . The denominator represents the ultimate tensile strength of the rebar which is calculated as the product of the minimum area for each bar from Table 2 multiplied by the average tensile strength. The numerator is the maximum load carried by the rebar during the test. The ratio should be less than or equal to one. Occasionally, the ratio is slightly greater than one. This occurs only when the mode of failure is due to tension failure of the rebar outside of the specimen and the strength of the rebar is slightly higher than the average value.

During tests, the slip at both ends of the bar increased with an increase in loading. In some specimens which failed by concrete splitting or bar pull out, the load vs. slip curves exhibited a descending portion; i.e., after the maximum load was reached, the bar would continue to slip while the load was reduced. As shown in Figure 6, the maximum slips reported in columns 6 and 7 of Tables 3 and 4 correspond to those measured at the maximum applied load.

One of the ways to compare the performance of different specimens is in terms of their stiffness. Because the service load stresses in GFRP rebars are expected to remain well below 50% of their ultimate strength, the initial stiffness,  $E_i$ , was defined as a secant modulus passing through the point of  $0.5 T_m^*$  (Figure 6). The values of initial stiffness are listed in Tables 3 and 4.

The modes of failure for the specimens included splitting failure of concrete (S), rebar pull out (P), and rebar fracture (R), as shown in Figures 7 through 9, respectively. The splitting failure is due to the small concrete cover which cannot

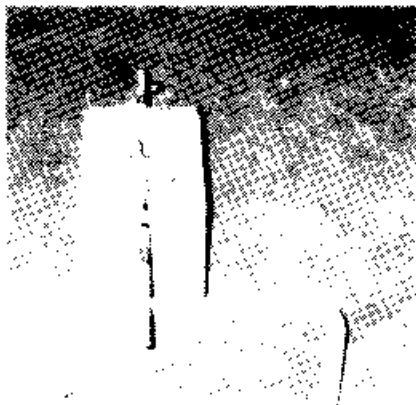


Figure 7. Failure of a specimen by tension splitting of the cover concrete.

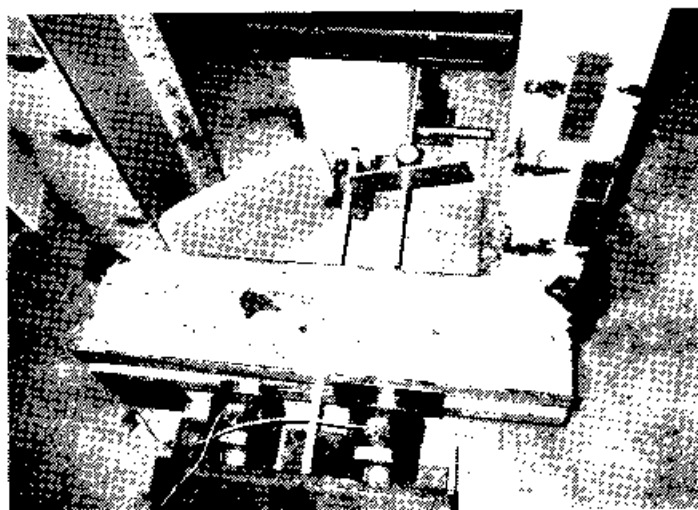


Figure 8. Failure of a specimen due to pull out of the rebar.



Figure 9. Failure of a specimen by fracture of the rebar between the grips and the concrete block.

sustain the circumferential tensile stresses (Park and Paulay, 1975). For shorter embedment lengths, the pull out failure happens when the slips at loaded and free ends increase rapidly with only a slight increase in the applied load. This signals the initial stage of a pull-out failure. If loading of the specimens is continued, the loads carried by the rebar will start to reduce rapidly. In contrast, under the conditions of longer embedment length and sufficient concrete cover, the load can be applied along the rebar until the rebar tensile stress reaches its ultimate strength. This is referred to as the rebar fracture mode.

#### Effect of Concrete Compressive Strength

The transfer of the applied load from the rebar to concrete is achieved through the bond mechanism which consists of three components: adhesion, bearing, and friction. Bond failure could be caused by tensile splitting and shearing of the concrete. In these cases, the tensile strength of concrete which is proportional to its compressive strength is considered a key parameter (ACI Committee 408, 1992). The selection of the concrete compressive strength at 28 and 56 MPa (4000 and 8000 psi) was intended to study the effect of this parameter on bond of GFRP rebars to concrete.

Splitting failure and rebar pull out are controlled by concrete strength and depth of cover, but rebar fracture is controlled by the tensile capacity of the rebars only. The ultimate bond stress for two pairs of beam specimens which did not fail by rebar fracture are presented here. The specimens in each pair had the same conditions except for different concrete strengths. The ultimate bond stress for these specimens were 46B12T2: 4.83 MPa (700 psi) and 86B12T2: 5.46 MPa (792 psi), and 49B22B2: 3.91 MPa (567 psi) and 89B22B2: 4.08 MPa (592 psi). As expected, for each pair, the ultimate bond stress increased with the increase in concrete compressive strength, although this increase was not proportional to

the square root of the concrete compressive strength. Similar behavior was observed in all other specimens which did not fail due to rebar fracture.

### Effect of Embedment Length

In order to obtain the lower limit for the required embedment length of GFRP rebars, the data from several specimens are compared in Figure 10. All data are presented for bottom bars in beam specimens constructed with 28 MPa (4000 psi) concrete. The embedment lengths tested for the three different bar diameters ranged as following: No. 3, 102 to 203 mm (4 to 8 in); No. 6, 76 to 457 mm (3 to 18 in); and No. 9, 102 to 762 mm (4 to 30 in). For each specimen, the ratio of the maximum applied load to the ultimate tensile force of the bar is plotted for various embedment lengths. Ideally, the embedment length should be large enough so that this ratio can reach 1.0. As shown in Figure 10, as the embedment length increases, the applied load does approach towards the tensile capacity of the rebar. However, none of the tested specimens had long enough development lengths to give a  $T_a^*/T_u$  equal to 1.

In absence of such data, the test results were extrapolated to estimate the required development length. Therefore, it is concluded that the minimum embedment length to develop the tensile capacity of No. 3, 6, and 9 rebars must be taken as 203, 457, and 762 mm (8, 18, and 30 in), respectively. Alternatively, the required development lengths can be expressed as 21, 24, and 27 times the bar diameter for No. 3, 6, and 9 rebars, respectively. Because the analysis of the above data was based on specimens with bottom bars, for top-cast rebars, the required embedment lengths should be multiplied by the top bar factor discussed later.

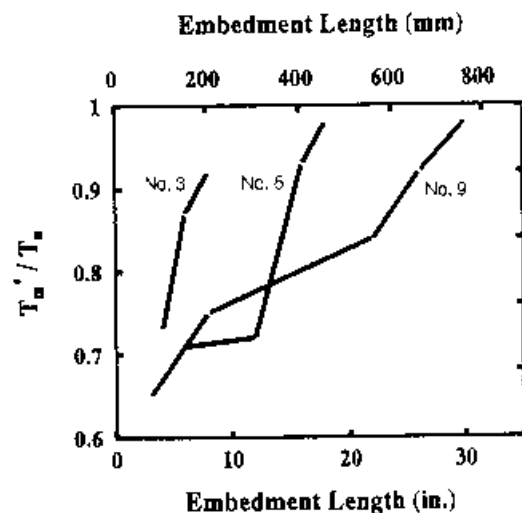


Figure 10. Ratio of maximum applied load to ultimate tensile force for different embedment lengths.

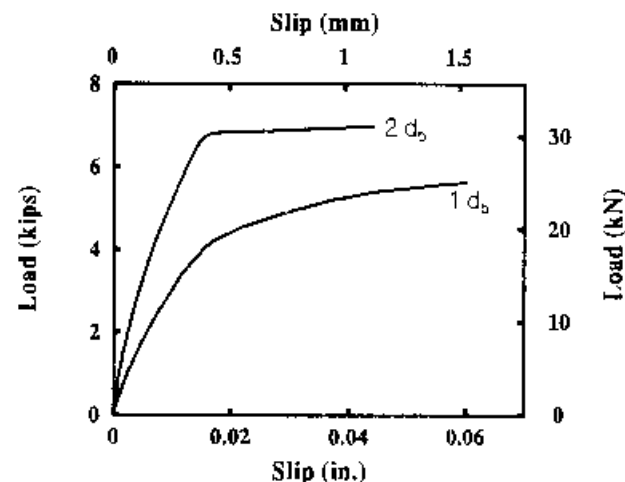


Figure 11. Initial stiffness and slip for different concrete covers.

### Effect of Clear Concrete Cover

The mode of failure observed during testing was strongly dependent on the clear concrete cover. In all specimens with a concrete cover of one rebar diameter, splitting failure occurred. When the cover concrete was twice the rebar diameter, depending on the embedment length, either bar pull out or rebar fracture was observed.

For a given embedment length, the ultimate bond stresses in specimens with a clear cover equal to twice the rebar diameter were larger than those for specimens with a clear cover of one rebar diameter. This is illustrated by comparing the bond stress of three pairs of specimens, where the only difference between the specimens in each pair was the concrete cover. The ultimate bond stress was 43B1.5T1: 21.85 MPa (3169 psi), and 43B1.5T2: 27.31 MPa (3961 psi); 46B3B1: 14.63 MPa (2122 psi) and 46B3B2: 18.73 MPa (2716 psi); and for the last pair, 49B4B1: 12.00 MPa (1740 psi) and 49B4B2: 17.07 MPa (2476 psi).

The comparison of Specimens 43B1.5T1 and 43B1.5T2 presented in Figure 11 indicates that smaller clear concrete cover results in lower initial stiffness and greater slip which is caused by the additional internal slip between concrete and rebar, permitted by the splitting cracks along the rebar (Ferguson, et al., 1965). The same trend was observed among all other similar specimens.

### Effect of Casting Position

The influence of casting position on the bond characteristics is significant. Three concrete depths of 203, 610, and 1016 mm (8, 24, and 40 in) were investigated in the pull out specimens, and in some of the beam specimens. Top rebars are defined as horizontal rebars so placed that more than 305 mm (12 in)

of concrete is cast below them (ACI Committee 318, 1995). Due to the bleeding of water and air trapped beneath the top rebars, the concrete surrounding these bars is less consolidated than that of bottom bars. For pull-out specimens cast with 28 MPa (4000 psi) concrete and No. 6 GFRP rebars (46PB6, 46PM6, and 46PT6), the data indicate that the higher the casting position, the lower the ultimate bond stress. However, the ultimate bond stress developed in specimens with a casting depth of 610 mm (24 in) and 1016 mm (40 in), 46PM6 and 46PT6, respectively, was nearly the same.

The poor quality of concrete surrounding the top bars also affected the slip of the bars during the test. Therefore, the initial stiffness of top rebars was lower than that of bottom bars, as shown in Table 4. The same general trend was noted for all specimens which failed either by tensile splitting of concrete or pull out of rebar. In the last column of Table 4, the ratios of  $u_m^*$  for bottom bars to that for the middle and top bars in each specimen are listed. As seen, these ratios range from 1.04 to 1.23 with an average of 1.13. Therefore, it is recommended that the provided embedment lengths for top bars should be at least 13% larger than that of bottom bars.

### Comparison of Beam and Pull-Out Specimens

There was a major difference between beam specimens and pull-out specimens. Both concrete and rebar in beam specimens were in tension. However, in pull-out specimens, the rebar was subjected to tension forces while the concrete surrounding the rebar was subjected to compression forces from the reaction of the jack. The latter conditions result in development lengths which are too short or unconservative.

As an example, the ultimate bond stress for Specimens 43B1, 5T2, 46B6B2, and 49B8B2 can be compared with Specimens 43PM1.5, 46PB6, and 49PB8 (see Tables 3 and 4). Due to the elimination of concrete flexural cracks in pull-out specimens, the ultimate bond stresses were increased by 3, 14, and 23 percent for No. 3, 6, and 9 rebars, and an average of 13 percent. This clearly indicates that reliance on data from pull-out tests for determination of development length can result in values which are unconservative. Beam test data would be more realistic and accurate for use in such calculations. Moreover, in pull-out specimens, the compressive stresses acting on the concrete surface limit the cracking of concrete and therefore reduce the slip at the loaded end. On the other hand, for beam tests, the tensile cracks in concrete contributed to the measured slip at the loaded end. As shown in Table 3, the loaded end slip for the above beam specimens were 1.13, 2.43, 5.03 mm (0.0443, 0.0956, and 0.1982 in), respectively. The slip for the pull-out specimens were 1.58, 4.35, 7.31 mm (0.0624, 0.1711, and 0.2876 in), respectively (see Table 4).

### CONCLUSIONS

The bond behavior of straight GFRP rebars was experimentally investigated with 48 beam and 18 pull-out specimens. The rebar sizes included in this study were No. 3, 6, and 9. The bond behavior of FRP rebars is greatly dependent on

the bar type and manufacturing process. For the bars investigated in this study, analysis of the test data led to the following conclusions:

1. When the failure is not governed by the fracture of the rebar, the ultimate bond stress increases with an increase in concrete compressive strength.
2. The applied tensile load approached the ultimate tensile capacity of rebars,  $f_u$ , as the embedment length increased.
3. For concrete compressive strength of 28 and 56 MPa (4000 and 8000 psi) investigated in this study, the embedment length for No. 3, 6, and 9 bottom rebars is approximately 21, 24, and 27 times bar diameters, respectively. For top rebars the above embedment length should be multiplied by the top bar factor of 1.13.
4. Splitting failure occurred when the clear concrete cover was one rebar diameter; pull out failure and rebar fracture modes were observed when the cover concrete was equal to or larger than twice the rebar diameter.
5. The ultimate bond stress and initial stiffness were found to increase with an increase in clear concrete cover for a given embedment length.
6. The ultimate bond stress and loaded end slip in pull-out specimens were significantly greater than the values observed in beam specimens. Therefore, beam test data are more realistic and accurate for use in determination of development length.

### ACKNOWLEDGEMENTS

The reinforcing bars used in this study were manufactured and donated by International Grating, Inc., Houston, Texas.

### NOMENCLATURE

$C_c$	clear concrete cover, in
$d_b$	rebar diameter, in
$E_i$	initial stiffness, kips/in
$f_c$	concrete compressive strength for each specimen, psi
$f'_{avg}$	average of $f_c$ for all 4,000 or 8,000 psi concrete, psi
$L$	bonded length of the rebar, in
$l_d$	embedment length, in
$S_{fmax}$	ultimate slip at free end, in
$S_{lmax}$	ultimate slip at loaded end, in
$T$	applied tensile load, kips
$T_m^*$	adjusted ultimate applied tensile load, kips
$T_u$	ultimate tensile capacity of rebar, kips
$u$	bond stress, psi
$u_m^*$	adjusted ultimate bond stress, psi
$\delta_e$	loaded end slip after correction for elastic elongation of rebar, in
$\delta_r$	elastic elongation of rebar, in
$\delta_w$	loaded end slip measured during testing, in

## REFERENCES

- ACI Committee 318. 1995. "Building Code Requirements for Structural Concrete (ACI 318-95) and Commentary (ACI 318R-95)." American Concrete Institute, Detroit, MI, p. 369.
- ACI Committee 408. 1992. "State-of-the-Art Report on Bond Under Cyclic Loads (ACI 408R-92)." American Concrete Institute, Detroit, MI, p. 32.
- ACI Committee 440. 1996. "State-of-the-Art Report on Fiber Reinforced Plastic Reinforcement for Concrete Structures (ACI 440R-96)." American Concrete Institute, Detroit, MI, p. 68.
- Chaalla, O., B. Benmakrane and R. Masmoudi. 1992. "An Innovative Glass-Fiber Composite Rebar for Concrete Structures." *Advanced Composite Materials in Bridges and Structures*, Canadian Society for Civil Engineering, pp. 169-177.
- Danali, S. 1992. "Development Length for Fiber-Reinforced Plastic Bars." *Advanced Composite Materials in Bridges and Structures*, Canadian Society for Civil Engineering, pp. 179-188.
- Ehsani, M. R. 1993. "Glass-Fiber Reinforcing Bars." in *Alternative Materials for the Reinforcement and Prepping of Concrete*, J. L. Clarke, ed., Blackie Academic & Professional, London, pp. 34-54.
- Ehsani, M. R., H. Saadatmanesh and S. Tao. 1993. "Bond of GFRP Rebars to Ordinary Strength Concrete." ACI International Symposium on Non-Metallic Continuous Reinforcement, Vancouver, Canada, pp. 333-345.
- Ehsani, M. R., H. Saadatmanesh and S. Tao. 1995. "Bond of Hooked Glass Fiber Reinforced Plastic (GFRP) Reinforcing Bars to Concrete." *ACI Materials J.*, 92(4):391-400.
- Ehsani, M. R., H. Saadatmanesh and S. Tao. 1996. "Design Recommendations for Bond of GFRP Rebars to Concrete." *J. of Struct. Eng. Div., ASCE*, 122(3):247-254.
- Faza, S. S. and H. V. S. GangaRao. 1990. "Bending and Bond Behavior of Concrete Beams Reinforced with Plastic Rebars." *Transportation Research Record* 1290, pp. 185-193.
- Ferguson, P. M. and J. N. Thompson. 1962. "Development Length of High-Strength Reinforcing Bars in Bond." *ACI J.*, 59(7):887-923.
- Ferguson, P. M., J. E. Breen and J. N. Thompson. 1965. "Pullout Tests on High Strength Reinforcing Bars." *ACI J.*, 62(8):933-949.
- Hadje-Ghaffari, H., O. C. Choi, D. Darwin and S. L. McCabe. 1992. "Bond of Epoxy Coated Reinforcement to Concrete: Cover, Casting Position, Slump, and Consolidation." *Structural Engineering and Engineering Materials*, SL Report 92-3, University of Kansas, Lawrence, KS.
- Kessler, R. J. and R. G. Powers. 1988. "Corrosion of Epoxy Coated Rebars: Keys Segmental Bridge, Monroe County." Report No. 88-8A, Florida Department of Transportation Materials Office, Corrosion Research Laboratory, Gainesville, FL.
- Pleinmann, L. G. 1987. "Tension and Bond Pull-Out Tests of Deformed Fiberglass Rods." Final Report for Marshall-Vega Corporation, Marshall, Arkansas. Civil Engineering Department, University of Arkansas, Fayetteville, AR, pp. 5-11.
- Pleinmann, L. G. 1991. "Strength, Modulus of Elasticity, and Bond of Deformed FRP Rods." *Advanced Composites Materials in Civil Engineering Structures*, Proceedings of the Specialty Conference, Materials Engineering Division, ASCE, pp. 99-100.
- Park, R. and T. Paulay. 1975. "Reinforced Concrete Structures." John Wiley & Sons, New York, pp. 401-404.
- Saadatmanesh, H. and M. R. Ehsani. 1991. "Fiber Composite Bar for Reinforced Concrete Construction." *J. of Composite Material*, pp. 188-203.
- Sen, R., D. Moriscal and M. Shahawy. 1993. "Durability of Fiberglass Prestensioned Beams." *ACI Structural Journal*, 90(5):525-533.
- Wu, W. P., H. GangaRao and J. C. Prucz. 1991. "Mechanical Properties of Fiber Reinforced Plastics." Research Report, Constructed Facilities Center, College of Engineering, West Virginia University.

## Effect of Heat Treatment on the Characteristics and Bond Behaviour of a SiC Reinforced Metal-Matrix Composite

M. MANI  
Division of Materials  
School of Applied Sciences  
Nanyang Technological University  
Singapore

M. GUNASEKARAN  
Department of Mechanical Engineering  
National University of Singapore  
Singapore

(Received October 1997)  
(Revised August 1998)

**ABSTRACT:** An understanding of the work hardening behavior of metal-matrix composites is crucial in the processing of these materials. The microstructure of metal-matrix composites can be altered by the choice of the heat treatment, which in turn determine the mechanical behavior of the composite. In this study, a reinforced aluminum metal matrix composite was used to study the effect of heat treatment on the work hardening behavior. The model was then used to relate the work hardening behavior to the microstructure. It is shown that the model is applicable for both

**KEY WORDS:** work hardening, aluminum matrix composite, interfacial properties, fracture strain.

### INTRODUCTION

THE DEVELOPMENT OF metal matrix composites (MMCs) for structural materials with high strength and stiffness requirements may be continuous in the form of whiskers or particulates. While fiber-reinforced composites provide specific stiffness along the reinforcement